Electronic Supplementary Information

Enhanced Hydrogen Evolution Activity of $CsPbBr_3$ Nanocrystals Achieved by Dimensionality Change

Qing Guo,*[,a] Jin-Dan Zhang,[a] Ya-Jing Chen,[b] Ke-Yuan Zhang,[a] Li-Na Guo,[a] Qi-Chao Shan,[a] Jun-Lin Lu,[a] Xin-Hua Duan*[,a] and Li-Zhu Wu[b]

[a]*Xi'an Key Laboratary of Sustainable Energy Material Chemistry, School of Chemistry, Xi'an Jiaotong University, Xi'an 710049, China.*

[b]*Key Laboratory of Photochemical Conversion and Optoelectronic Materials, Technical Institute of Physics and Chemistry, Chinese Academy of Sciences, Beijing 100190, China*

*To whom correspondence should be addressed.

E-mail: guoqing92@xjtu.edu.cn; duanxh@xjtu.edu.cn

Table of Contents

1. Materials

Lead bromide ($PbBr_2$, 99%), Cesium carbonate (Cs_2CO_3, 99.9%), tetrafluoroborate amine (NH_4BF_4, 98%), tetrabutylamine hexafluorophosphate ($TBAPF_6$, 99.9%), oleylamine (OAm approximate, C18-content 90%+) and oleic acid (OA, 90%+) were purchased from Adamas-beta and used as received. Octadecene (ODE, >90.0%) was obtained from Aladdin and used as received. Other chemicals are of analytical grade without any further purification unless otherwise noted.

2. Instruments

High-resolution transmission electron microscopy (HRTEM) was performed by JEM 2100F (operated at an accelerating voltage of 200 kV). Energy-dispersive X-ray (EDX) and elemental mapping were performed by Talos F200X. The X-ray photoelectron spectra (XPS) measurements were conducted on an ESCALAB 250 spectrophotometer with Al-Kα radiation. And the binding energy scale was using C 1s peak at 284.6 eV. X-ray powder diffraction pattern (XRD) was performed on a Bruker AXS D8 X-ray diffractometer (parameters: Cu Kα, λ = 1.5406 Å, 100 mA, and 40 kV), and the $CsPbBr_3$ samples dispersed in hexane were droped on the surface of ITO and measured. UV-vis spectra and steady-state photolumesience (PL) spectrum for $CsPbBr_3$ hexane solution were obtained from Lambd950 and LS-55, respectively, in which $CsPbBr_3$ nanocrystals without ligand exchange. Photolumesience (PL) spectrum and time-resolved PL decay curves for $CsPbBr_3$ powers capped with BF_4^- were obtained on a FLS-920 fluorescence lifetime spectrophotometer (Edinburgh Instruments, UK) under the excitation of 405 nm and probed at 520 nm. Fourier transform infrared spectroscopy (FT-IR) spectra were performed on FT-IR spectrometer (Nicolet iS50) with a KBr disk containing $CsPbBr_3$. Zeta potential was measured by the Nano-ZS zetasizer.

3. Synthesis of Cs-oleate solution: Cs-oleate solution was synthesized by reported methods.[1, 2] Briefly, 346.2 mg (1.0625 mmol) Cs_2CO_3 and 2.5 mL OA were placed in a 3-neck flask containing 6.0 mL ODE. The solution was degassed under vacuum for 30 min. Then the flask was filled with highly pure nitrogen (N_2) and heated to 150 ^oC by heating mantle under magnetic stirring until all Cs_2CO_3 dissolved.

4. Synthesis of 3D $CsPbBr_3$ nanocubes: 207 mg (0.564 mmol) $PbBr_2$ and 15.0 mL ODE were loaded into a 3-neck flask and degassed under vacuum for 30 min. The flask was filled with N_2 and heated to 120 °C. Then 1.5 mL OA and 1.5 mL OAm were injected swiftly under N_2. The temperature was raised to 170 °C to allow the complete dissolution of $PbBr_2$. Then 1.2 mL as-prepared Cs-oleate solution was quickly injected under N_2. After 5 s, the reaction mixture was cooled by ice-water bath. After the solution was cooled down to room temperature, the product was obtained by centrigfugation and washed with hexane twice. And finally dried at 60 °C under vacuum.

5. Synthesis of 1D $CsPbBr_3$ nanorods: 207 mg (0.564 mmol) $PbBr_2$ and 15.0 mL ODE were loaded into a 3-neck flask and degassed under vacuum for 30 min. The flask was filled with N_2 and heated to 120 °C. Then 1.5 mL OA and 1.5 mL OAm were injected swiftly under N_2. The temperature was raised to 150 ℃ and kept for 1 h to allow the complete dissolution of $PbBr_2$.[1] Then 1.2 mL as-prepared Cs-oleate solution was quickly injected under N_2. After 90 min, the reaction mixture was cooled by ice-water bath. After the solution was cooled down to room temperature, the product was obtained by centrifugation and washed with hexane twice. And finally dried at 60 ℃ under vacuum.

6. Ligand exchange: ligand exchange was performed according to a previous method.[3] Briefly, 250 mg above obtained $CsPbBr_3$ nanocrystals were dispersed in 25.0 mL ethyl acetate. And 25.0 mg NH_4BF_4 was dispersed in 1.0 mL ethanol. Under vigorously stir, NH_4BF_4 was slowly dropped into prepared $CsPbBr_3$ ethyl acetate solution. After 30 min stirring under dark, the long-chain organic ligands on $CsPbBr_3$ surface were removed by BF_4^-. And $CsPbBr_3$ capped with BF_4^- was obtained by centrifuging at 6500 rpm for 6 min and dried at 60 ℃ under vacuum.

7. Photocatalytic hydrogen production: the solar H_2 generation reaction was conducted in a closed glass reaction system (CEL-SPH2N, CEAULIGHT, Beijing). First of all, 100.0 mg photocatalyst $CsPbBr_3$ samples were added into 10.0 mL hydrobromic acid (HBr) aqueous solution and stirred to allow dynamic equilibrium of the dissolution and precipitation of $CsPbBr_3$ in saturated aqueous solutions. Then, 2.5 mL hypophosphite (H_3PO_2) was added to act as reducing agent for Br_3^- to Br- reaction. Certain volume of H_2PtCl_6 aqueous solution (c = $1mg_{Pt}$/mL) was added as cocatalyst. After that the air in reactor was evacuated using a vacuum pump for 30

min. Subsequently, the reactor was irradiated by a 300 W Xe lamp with a cut-off filter of 400 nm. The generated molecular H_2 in the reactor system was measured using an online gas chromatograph system (*Shimadzu* GC2014CAFC/APC) equipped with a thermal conductivity detector and a 5 Å molecular sieves GC column. Ar was used as a carrier gas. Error bars on H_2 were calculated from at least three independent experiments.

For optimization mass ratios of Pt to $CsPbBr_3$, the volume of H_2PtCl_6 solution was 0.2 mL, 0.5 mL, 1.0 mL and 1.5 mL for 0.2 wt %, 0.5 wt %, 1.0 wt % and 1.5 wt %, respectively, and other procedures were similar to above.

For the wavelength-dependent activities were measured using a bandpass filter of 400 nm, 450 nm, 520 nm, and 600 nm, respectively, instead of cut-off filter of 400 nm and other procedures were similar to above.

8. The measurement of apparent quantum yield (AQY): Briefly, the mixture of 60.0 mL hydrobromic acid (HBr), 15.0 mL hypophosphoric acid (H_3PO_2) and 6.0 mL H_2PtCl_6 solution containing 600.0 mg photocatalyst 1D NRs was placed in a sealed photoreactor with a round irradiation surface (**Fig. S15**). And the diameter of irradiation surface is 7.0 cm. Then, the system was irradiated under Xe lamp (λ = 450 nm, P = 3000 μW · cm^{-2}). The evolved H_2 gas during 8.0 h was analyzed by GC. As a result, the number of absorbed photons could be calculated as the following equation:

$$N_{photon} = \frac{t(s) \times P(W \cdot cm^{-2}) \times S(cm^2) \times \lambda(m)}{h(J \cdot s) \times c(m \cdot s^{-1})}$$

$$= \frac{8 \times 3600(s) \times 3 \times 10^{-3}(W \cdot cm^{-2}) \times \pi \times 3.5^2(cm^2) \times 450 \times 10^{-9}(m)}{6.626 \times 10^{-34}(J \cdot s) \times 3 \times 10^{8}(m \cdot s^{-1})}$$

$$= 7.5 \times 10^{21}$$

So the apparent quantum yield (AQY) of photocatalytic H_2 evolution was calculated as following equation:

$$AQY = \frac{2n(H_2) \times 6.02 \times 10^{23}}{N_{photon}} \times 100\%$$

For 1D NRs system, about 2.56 μmol molecular H_2 was produced in 8.0 h. Herein, the AQY can be calculated as follows:

$$AQY = \frac{2 \times 2.56 \times 10^{-6}(\text{mol}) \times 6.02 \times 10^{23} / mol}{7.5 \times 10^{21}} \times 100\%$$

$$= 0.04\%$$

9. Photoelectrochemical measurements: all experiments were performed on an electrochemical workstation (Shanghai Chenhua, China) in a conventional three-electrode system. The resultant electrode served as the working electrode, platinum as the counter electrode and Ag/AgCl (3.0 M KCl) electrode as the reference electrode. A 0.1 M $TBAPF_6$ acetonitrile solution was used as the electrolyte. The working electrodes were prepared by adding 10 μL Nafion (5%) aqueous solution into a 1 mL $CsPbBr_3$ ethyl acetate solution. Then 80.0 μL obtained solution was dropped onto a clean ITO conductive glass with an active area of about 1.0 cm^2, which was cleaned before experiments by ultrasonication with distilled water, ethanol and isopropanol for 15 s, and dried in a vacuum. The obtained electrode was dried at 40 ^oC under vacuum. The photocurrent response versus time (I-t curve) was recorded in the above three-electrode system with 300 W Xe lamp ($\lambda \geq 400$ nm) as the light source under visible light switching on and off mode. The electrochemical impedance spectroscopy (EIS) results were recorded at the open circuit potential using a frequency ranged from 10^5 Hz to 10^{-1} Hz. The polarization curves were recorded in the same three-electrode system and the bias sweep range was from -1.0 to 0 V versus Ag/AgCl with a step size of 0.001 V.

10. DFT calculations

Details: the DFT calculations were performed by the CASTEP package[4] with the ultrasoft pseudopotentials[5] and GGA-PBE functional.[6, 7] A 550 eV plane wave basis set the cutoff, and the cutoff energy was used throughout our calculations. The convergence thresholds between optimization cycles for energy change and maximum force were set as 5.0×10^{-6} eV/atom and 0.03 eV/Å, respectively. First, the structural optimization was performed. The optimized lattice constant is a=8.463 Å, b=11.7294 Å, c=7.91 Å, which is consistent with experimental data (a=8.244 Å, b=11.735 Å, c=8.098 Å). Then, based on the optimized orthorhombic bulk lattice, a (010) slab was built. A vacuum thickness of 13 Å was added to avoid the interaction of adjacent

layers. For $CsPbBr_3$ model with Br vacancies, one or two Br atoms were removed from the first-layer of (010) surface. The Monkhorst-Pack grids[8] of 3×3×1 *k*-points were used for the $CsPbBr_3$ (010) facet. In all calculations, the atoms in the bottom layers were fixed, but the atoms in the three topmost layers, as well as H atoms, were allowed to be relaxed.

The adsorption energy and Gibbs energy ΔG was defined as,

$$\Delta G = E_{ads} + \Delta ZPE - T\Delta S,$$

in which $\Delta ZPE - T\Delta S$ can be assumed as 0.24 eV[9, 10] for H atom and

$$E_{ads} = E_{(H+slab)} - [\frac{1}{2}E_{(H_2)} + E_{(slab)}],$$

where the first term is the total energy of the slab with the adsorbed H^+ on the surface, the second term is the total energy of isolated H_2 molecule, and the third term is the total energy of the bare slab of the surface. According to the above definitions, a negative E_{ads} value corresponds to an exothermic adsorption, and the more negative the E_{ads}, the stronger the adsorption.

11. Comparison of the charge-carrier behaviors

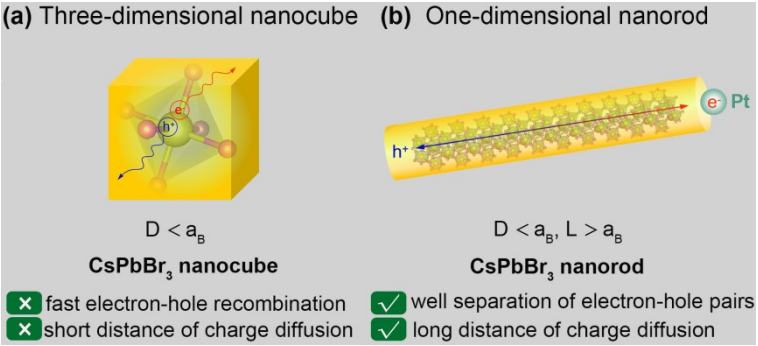

Scheme S1. Comparison of the charge-carrier behaviors in (a) 3D $CsPbBr_3$ nanocube and (b) 1D $CsPbBr_3$ nanorod upon incident photon excitation, in which D represents the size or diameter of nanocube or nanorod, L is the length of nanorod, and a_B is the Bohr exciton diameter.

12. XRD pattern of $CsPbBr_3$

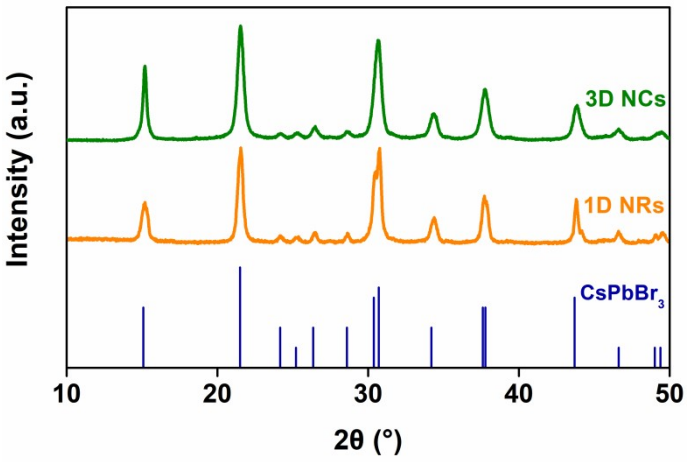

Fig. S1 XRD pattern of obtained $CsPbBr_3$ nanocubes and nanorods, respectively.

13. Size distribution statistics of 3D NCs

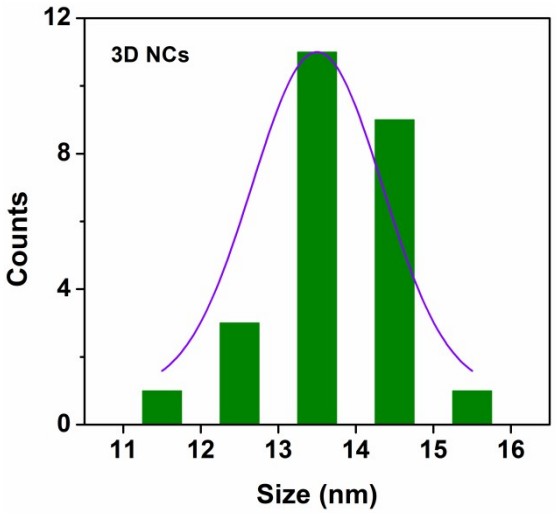

Fig. S2 The average size of obtained 3D NCs. As shown in Fig. S2, the size of 3D NCs is around 13~14 nm.

14. The lattice distances of (001) facet of 3D NCs

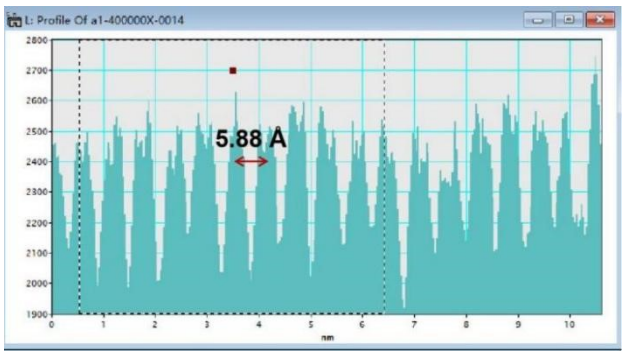

Fig. S3 The corresponding lattice distances of the exposed (001) plane of 3D NCs in Fig. 1b.

15. Diameter distribution statistics of 1D NRs

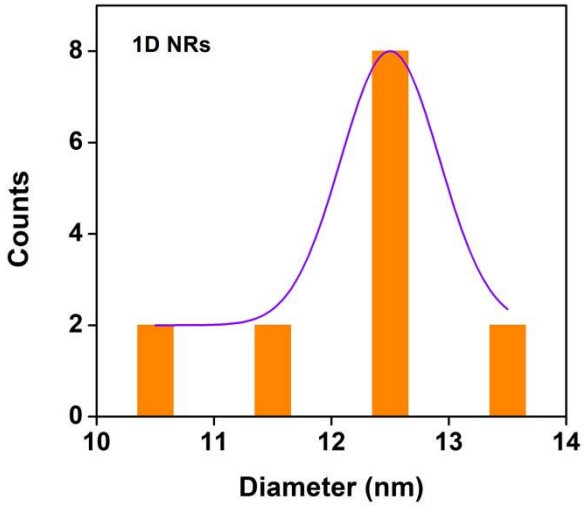

Fig. S4 The average diameter of obtained 1D NRs. As shown in Fig. S4, the diameter of 1D NRs is around 12~13 nm.

16. The lattice distance of (001) facet of 1D NRs

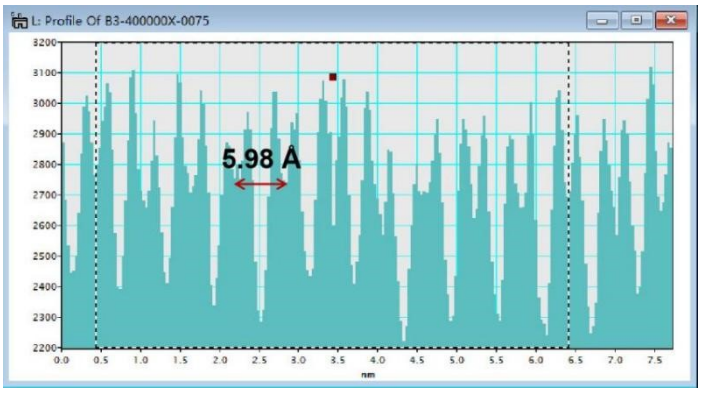

Fig. S5 The corresponding lattice distance of the exposed (001) plane of 1D NRs in Fig. 1e.

17. EDX spectrum of $CsPbBr_3$

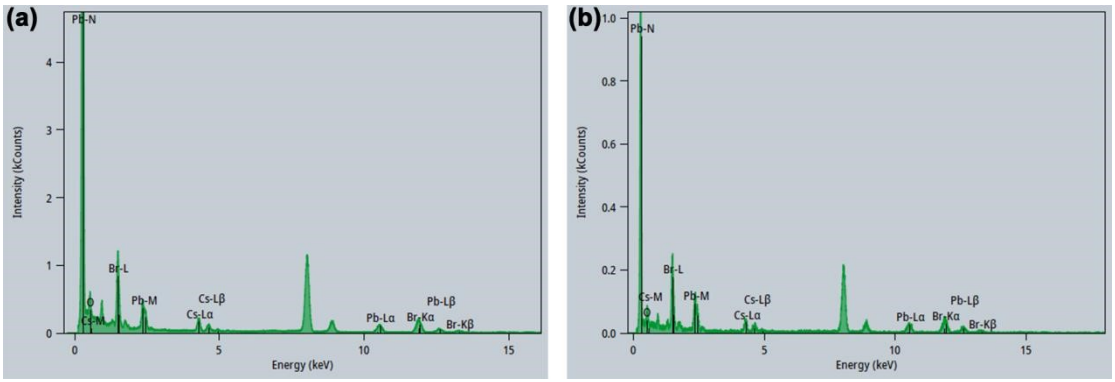

Fig. S6 EDX spectrum of obtained 3D NCs (a) and 1D NRs (b), respectively, revealing the coexistence of Cs, Pb and Br elements.

18. Full XPS spectra of $CsPbBr_3$

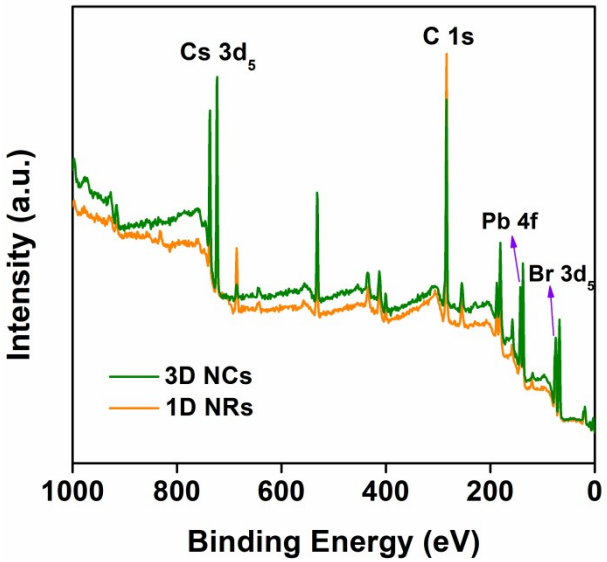

Fig. S7 Full XPS spectra of the obtained 3D NCs and 1D NRs, respectively, indicating that Cs, Pb and Br elements are found in the spectra.

19. UV-vis absorption spectra of obtained $CsPbBr_3$ nanocrystals

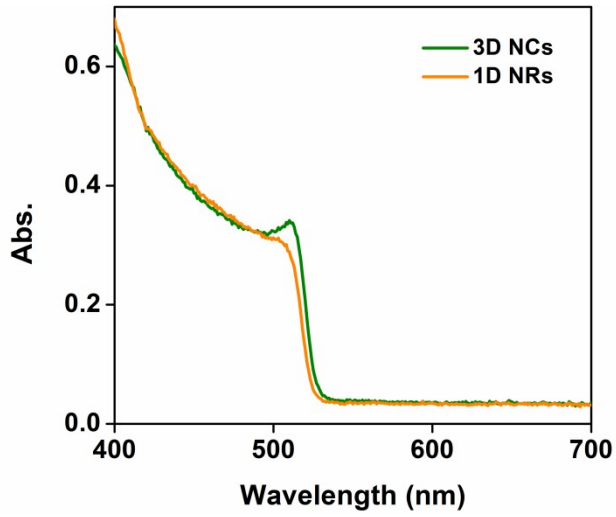

Fig. S8 UV-vis absorption spectra of 3D NCs and 1D NRs in hexane solution at room temperature, respectively.

20. PL spectrum of obtained $CsPbBr_3$ nanocrystals

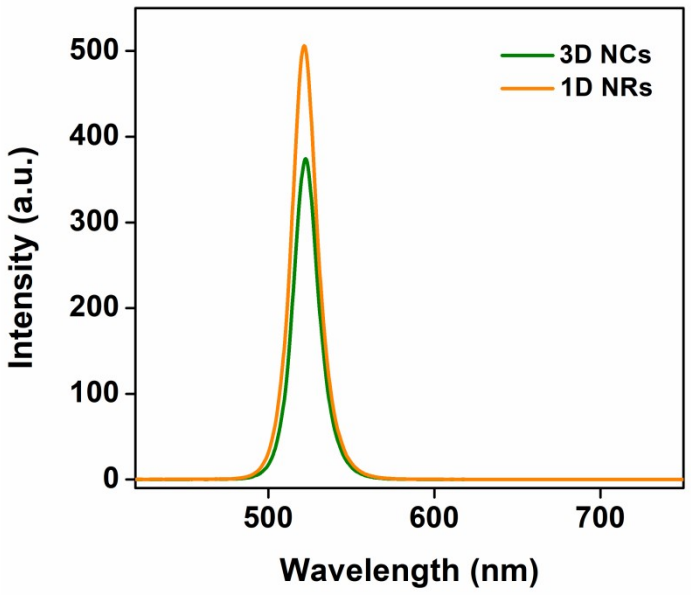

Fig. S9 PL spectrum (excitation: 400 nm laser) of 3D NCs and 1D NRs in hexane solution at room temperature, respectively.

21. IR spectra of $CsPbBr_3$ before and after ligand exchange

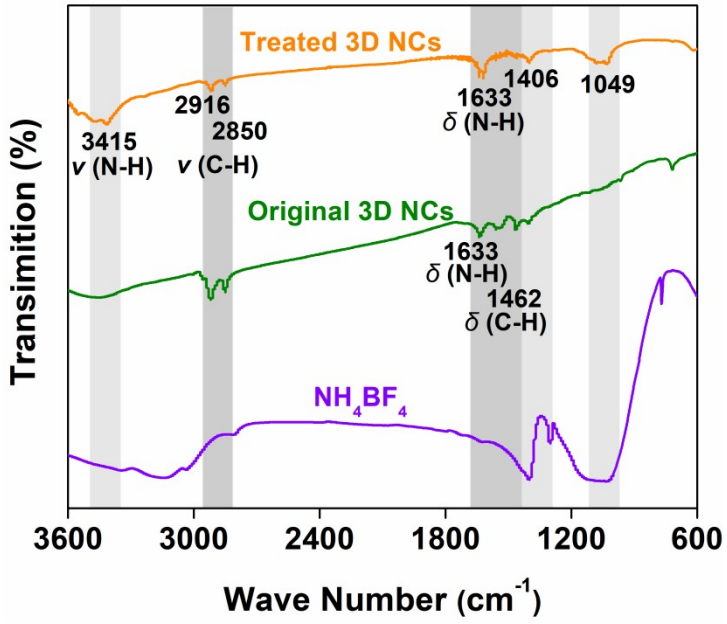

Fig. S10 The Fourier transform-infrared (FT-IR) spectra of $CsPbBr_3$ nanocubes before (denoted as original 3D NCs) and after ligand exchange (denoted as treated 3D NCs). As shown in Fig. S10, after ligand exchange, the intensity of peaks at 2916 cm^{-1}, 2850 cm^{-1} and 1462 cm^{-1}, which were attributed to vibration of C-H bond of long-chain organic ligands, was reduced, indicating the success of ligand exchange from long-chain organic ligands to BF_4^- ions.[3]

22. Table S1. BET surface areas and normalized H_2 rates of nanocube and nanorod

Sample	BET surface area ($m^2 \cdot g^{-1}$)	H_2 rate ($\mu mol \cdot m^{-2}$)
3D nanocube	0.402	19.9
1D nanorod	0.316	79.1

23. Photocatalytic efficiency with the mass ratio of Pt to $CsPbBr_3$

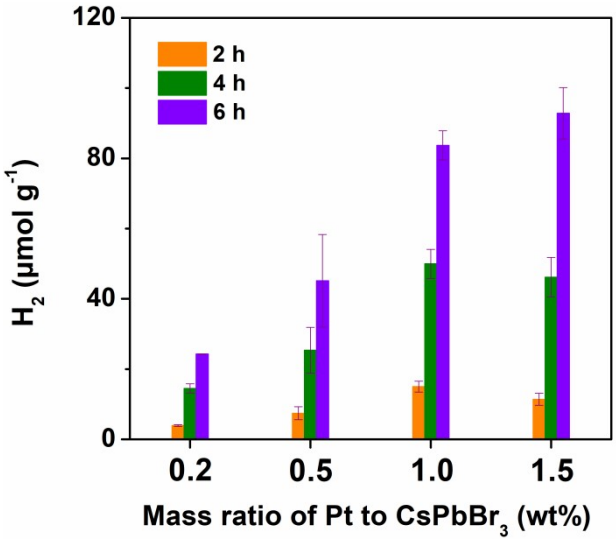

Fig. S11 The variation of solar H_2 evolution with different mass ratios of Pt to $CsPbBr_3$. As shown in Fig. S11, gradually increasing the mass ratio of Pt from 0.2 wt% to 1.0 wt% could significantly improve the rate of H_2 evolution. However, with further increase of Pt to 1.5 wt%, H_2 generation rate enhanced slower. From the economic perspective, we chose 1.0 wt% as the optimal mass ratio.

24. H_2 evolution activity under AM 1.5 irradiation

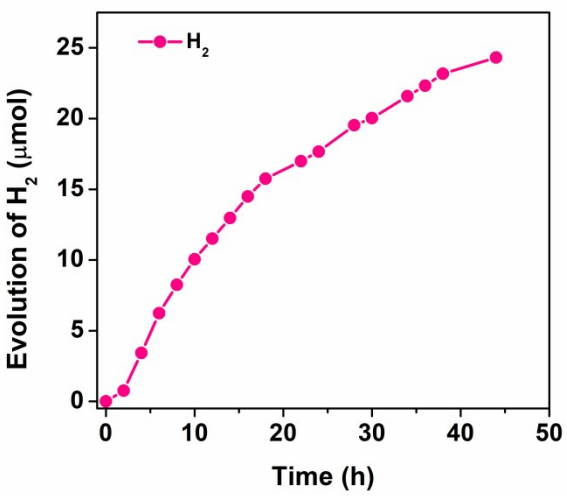

Fig. S12 Photocatalytic H_2 evolution of 1D NRs with long-time irradiation under AM 1.5.

25. XRD pattern of recycled 1D NRs

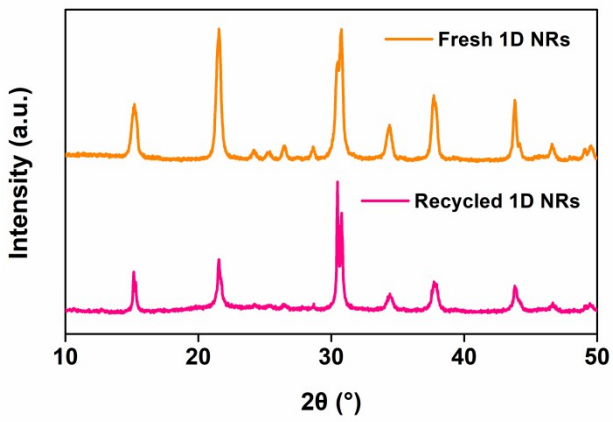

Fig. S13 XRD patterns of fresh and recycled 1D NRs.

26. TEM image of recycled 1D NRs

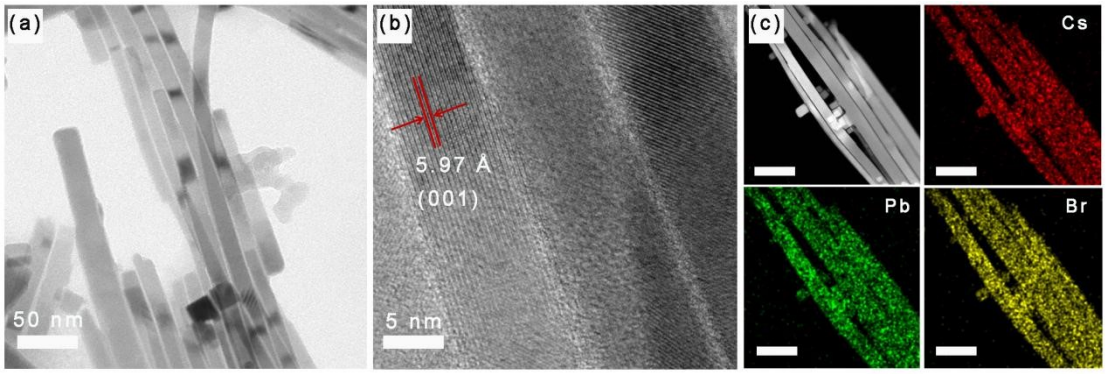

Fig. S14 (a) TEM image, (b) high-resolution TEM image of recycled 1D NRs and (c) corresponding elemental mapping of Cs, Pb and Br elements, respectively, over recycled 1D NRs.

26. The illustration of used photoreactor for AQY measurement

Fig. S15 Schematic illustration of the photoreactor used in our system for AQY measurement.

28. Wavelength-dependent activity of 1D NRs for H_2 production

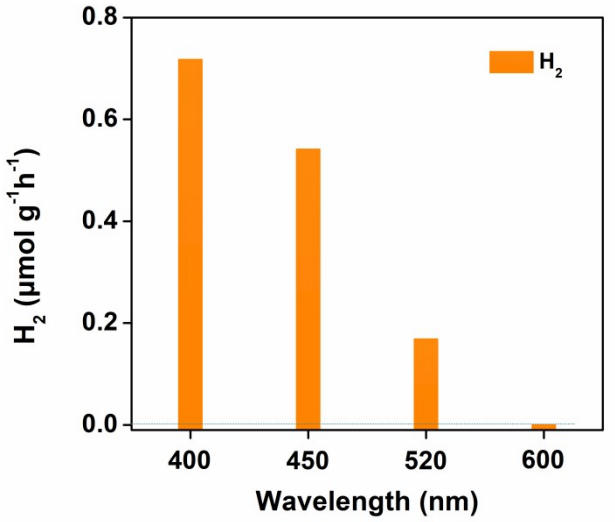

Fig. S16 Wavelength-dependent activity of 1D NRs for H_2 generation.

29. XRD pattern of other samples with varied reaction time

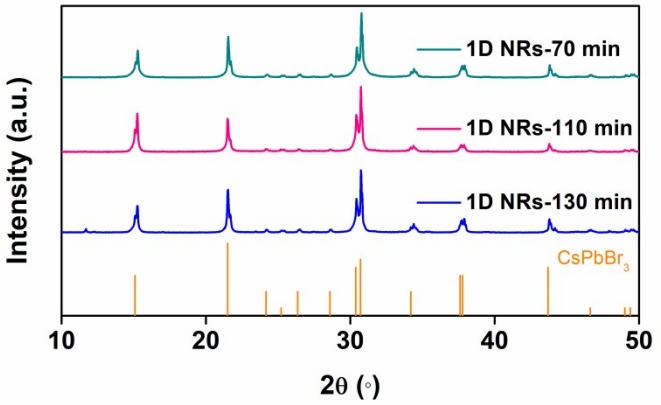

Fig. S17 XRD pattern of obtained samples with reaction time of 70 min, 110 min and 130 min, respectively.

30. TEM image of obtained samples with varied reaction time

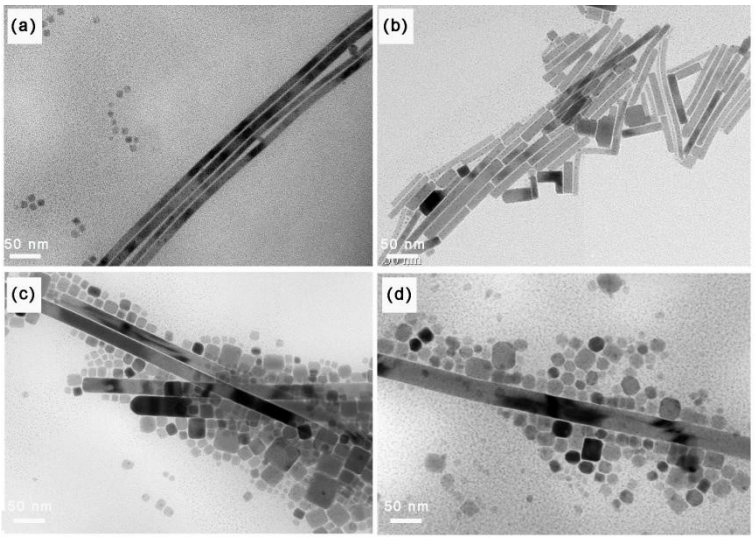

Fig. S18 TEM image of obtained samples with reaction time of (a) 70 min, (b) 90 min (1D NRs in our work), (c) 110 min and (d) 130 min, respectively.

30. Comparison of H_2 evolution activity of 1D NRs with other obtained samples

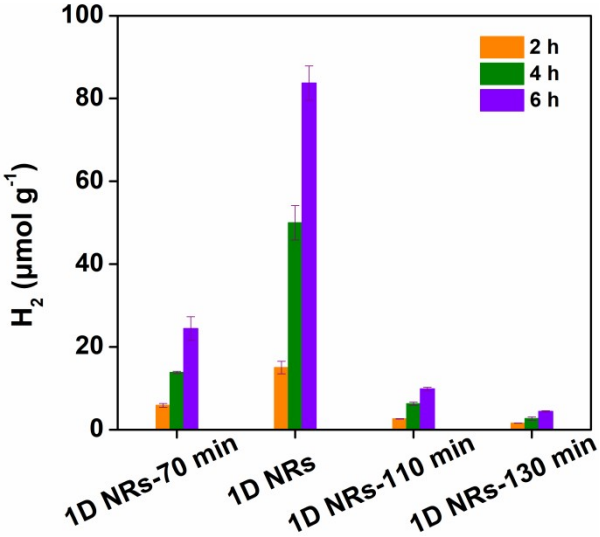

Fig. S19 H_2 evolution activities of obtained samples with reaction time of (a) 70 min (1D NRs-70 min), (b) 90 min (1D NRs), (c) 110 min (1D NRs-110 min) and (d) 130 min (1D NRs-130 min), respectively.

32. XRD pattern of synthesized other perovskites

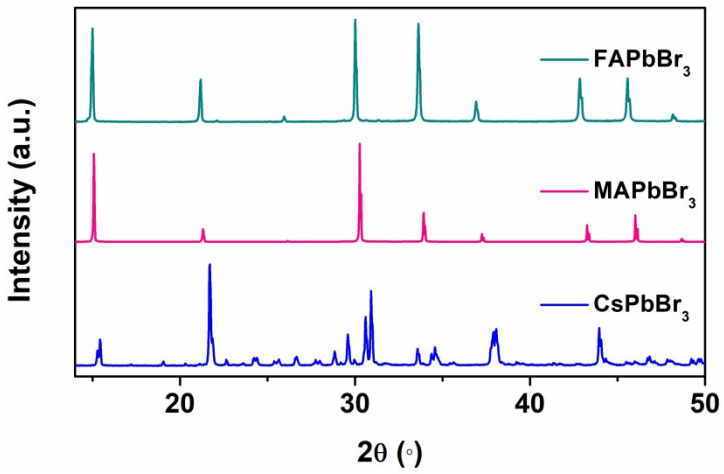

Fig. S20 XRD pattern of synthesized $FAPbBr_3$, $MAPbBr_3$ and $CsPbBr_3$ by anti-solvent precipitation method.[11-13]

33. Table S2. Comparison of H_2 evolution activity with $FAPbBr_3$, $MAPbBr_3$ and $CsPbBr_3$

Samples	Light	The amount of catalyst (g)	Irradiation time (h)	H_2 evolution (μmol)	H_2 evolution rate (μmol $g^{-1}h^{-1}$)
$FAPbBr_3$	λ ≥ 400 nm	1.0	6.0	49.5	8.2
$MAPbBr_3$	λ ≥ 400 nm	1.0	6.0	11.2	1.9
$CsPbBr_3$	λ ≥ 400 nm	1.0	6.0	4.3	0.7
1D NRs	λ ≥ 400 nm	1.0	6.0	1.0	0.2
		0.1 **(our work)**	6.0	8.4	14

Photocatalytic experiments were conducted under identical conditions as 1D NRs in our work, in which 100 mg catalysts were added into 10.0 mL HBr with 2.5 mL H_3PO_2 and 1.0 mL H_2PtCl_6. However, because of the lack of surface ligands, the solubility of above obtained perovskite materials in HBr aqueous solution is superior to that of 1D NRs in our work, leading to colorless and transparent solution after 100.0 mg materials added into 10.0 mL HBr, which is quite different from 1D NRs in our work. So that photocatalytic system was changed to 1.0 g materials added into 4.0 mL HBr with 1.0 mL H_3PO_2 and 400 μL H_2PtCl_6. After 6.0 h irradiation under Xe lamp (λ ≥ 400 nm), H_2 evolution was detected by GC. As shown in **Table S2**, $FAPbBr_3$ exhibited highest activity of 8.2 μmol $g^{-1}h^{-1}$, while 1D NRs shown lowest activity of 0.2 μmol $g^{-1}h^{-1}$. The poor activity is mainly owing to the serious light scattering, which resulted from the low solubility of 1D NRs with surface ligands leading to the much more suspended particles after 1.0 g 1D NRs added into 4.0 mL HBr. In order to reduce light scattering, we changed the amount of 1D NRs to 0.1 g, and found that 1D NRs in our work exhibited highest activity of 14 μmol $g^{-1}h^{-1}$ among $FAPbBr_3$, $MAPbBr_3$ and $CsPbBr_3$.

34. XPS valence-band spectra of $CsPbBr_3$

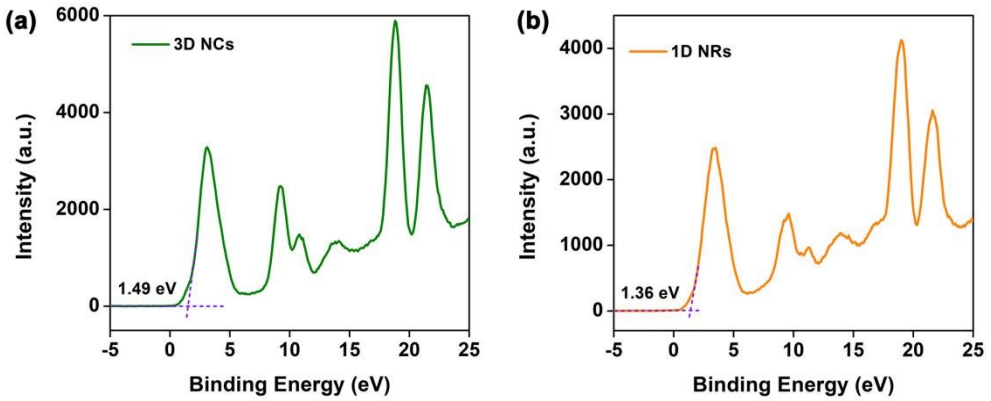

Fig. S21 XPS valence-band spectra of (a) 3D NCs and (b) 1D NRs, respectively. As shown in Fig. S21, 3D NCs give a valence band position of ~+1.49 V *vs* NHE, which is more positive than that of 1D NRs with ~+1.36 V *vs* NHE.

35. The corresponding *Tauc* plots of $CsPbBr_3$

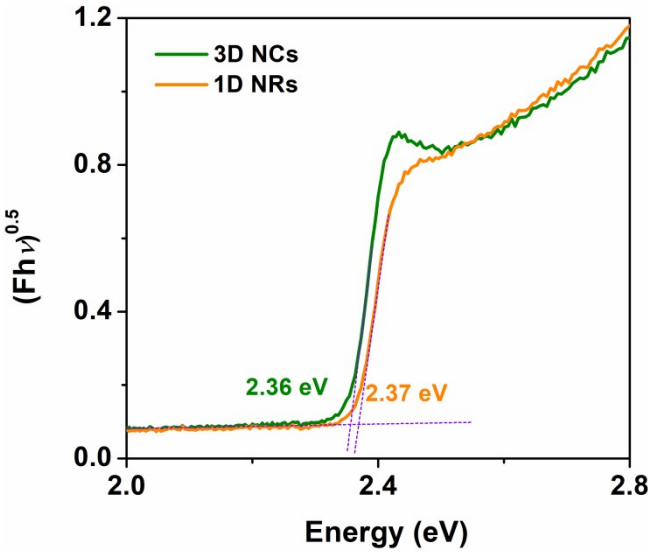

Fig. S22 The corresponding *Tauc* plot of 3D NCs and 1D NRs, from which we can find that 3D NCs and 1D NRs could give a band gap of ~2.36 and ~2.37 eV, respectively.

36. Band structure diagram of $CsPbBr_3$

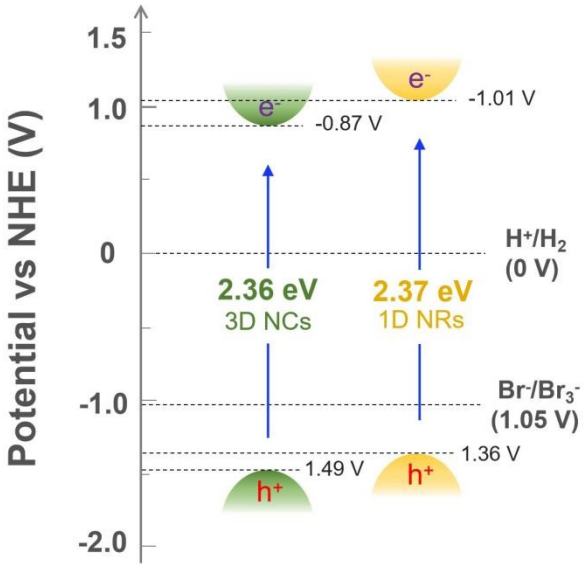

Fig. S23 Schematic illustration for the band structure of 3D NCs and 1D NRs. As shown in Fig. S23, it is thermodynamically feasible for the proton reduction reaction on both 3D NCs and 1D NRs.

37. Table. S3 Fitted parameter of PL lifetime in Fig. 3b

Samples	B_1	B_2	τ_1 / ns	τ_2 / ns	τ / ns
3D NCs	2192.03	268.46	24.56	152.60	79.89
1D NRs	1845.73	155.33	24.17	244.63	125.57

The emission decay of $CsPbBr_3$ nanocubes and nanorods were studied and the decay curves for the samples were well fitted with double-exponential function *Y*(t) based on nonlinear least-squares, using the following equation:

$$Y(t) = B_1 \exp(-t / \tau_1) + B_2 \exp(-t / \tau_2)$$

Where B_1, B_2 are fractional contributions from time-resolved emission decay lifetime τ_1, τ_2, as shown in Table S3. The average lifetime τ could be obtained from the following equation:

$$< \tau >= \frac{B_1 \tau_1^2 + B_2 \tau_2^2}{B_1 \tau_1 + B_2 \tau_2}$$

38. Table S4. Fitted equivalent circuit of 3D NCs and 1D NRs

Samples	Rs/Ω	Rct/Ω
3D NCs	22.72	1456
1D NRs	14.27	778

39. The polarization curves of $CsPbBr_3$

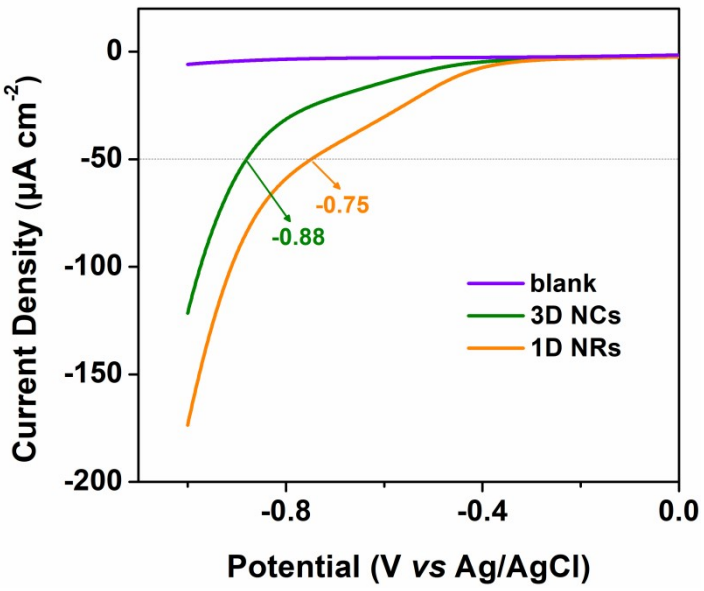

Fig. S24 The polarization curves of 3D NCs and 1D NRs electrodes. As shown in Fig. S24, 1D NRs shows a lower overpotential of -0.75 V (*vs* Ag/AgCl) than 3D NCs at 50 μA cm^{-2}, indicating that dimensionality tuning at morphology level can decrease the overpotential and promote proton reduction to H_2.

40. High resolution XPS signals of Pb 4f of $CsPbBr_3$

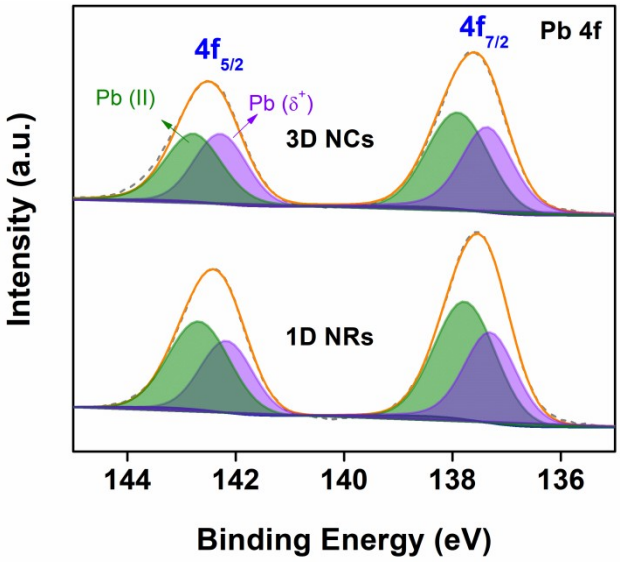

Fig. S25 High resolution XPS signals of Pb 4f of 3D NCs and 1D NRs.

41. Table S5. Summary of integrated areas of fitting peaks of Pb elements from XPS analysis

Samples	Areas of Pb element				Ratios of Pb (δ^+)/%
	Pb $4f_{5/2}$		Pb $4f_{7/2}$		
	Pb (II)	Pb (δ^+)	Pb (II)	Pb (δ^+)	
3D NCs	56388.01	48963.52	78316.67	67073.3	46.3
1D NRs	37868.29	26198.11	50491.05	35887.82	41.3

42. Table S6. Zeta potentials of the 3NCs and 1D NRs

Samples	Zeta potential (mV)
3D NCs	-10.0
1D NRs	-3.42

43. The corresponding structural models of H atom adsorption

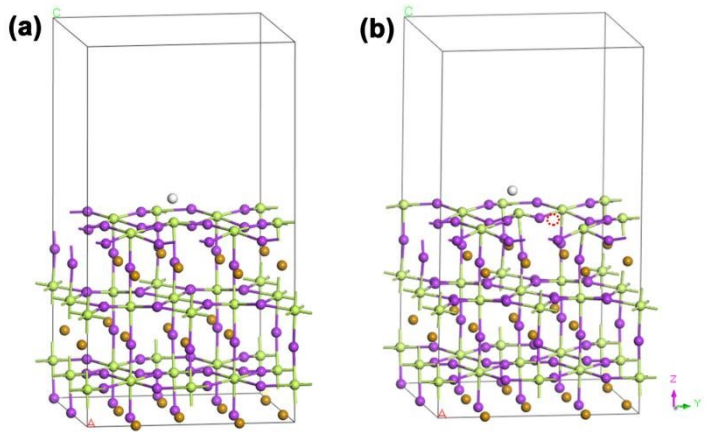

Fig. S26 Structural models of H atom adsorption on (a) perfect $CsPbBr_3$ (denoted as *P* $CsPbBr_3$) and (b) $CsPbBr_3$ with Br vacancy (denoted as V_{Br} $CsPbBr_3$). The yellow, green and purple balls represent Cs, Pb and Br atoms, respectively, and red circle represents Br vacancy.

44. The calculated free-energy diagram of H_2 evolution reaction

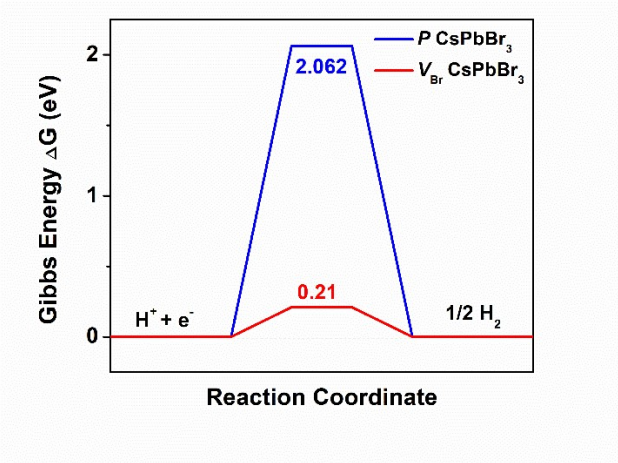

Fig. S27 The calculated free-energy diagram of H_2 evolution reaction at the equilibrium potential (U = 0 V) on the surfaces of the perfect $CsPbBr_3$ (*P* $CsPbBr_3$) and $CsPbBr_3$ with Br vacancy (V_{Br} $CsPbBr_3$) model, respectively.

45. References

1. D. Zhang, Y. Yu, Y. Bekenstein, A. B. Wong, A. P. Alivisatos and P. Yang, *J. Am. Chem. Soc.*, 2016, **138**, 13155-13158.

2. L. Protesescu, S. Yakunin, M. I. Bodnarchuk, F. Krieg, R. Caputo, C. H. Hendon, R. X. Yang, A. Walsh and M. V. Kovalenko, *Nano Lett*, 2015, **15**, 3692-3696.

3. J.-C. Wang, N. Li, A. M. Idris, J. Wang, X. Du, Z. Pan and Z. Li, *Solar RRL*, 2021, **5**.

4. S. J. Clark, M. D. Segall, C. J. Pickard, P. J. Hasnip, M. J. Probert, K. Refson and M. C. Payne, *Zeitschrift Fur Kristallographie*, 2005, **220**, 567-570.

5. D. Vanderbilt, *Phys. Rev. B*, 1990, **41**, 7892-7895.

6. M. C. Payne, M. P. Teter, D. C. Allan, T. A. Arias and J. D. Joannopoulos, *Rev. Mod. Phys.* , 1992, **64**, 1045-1097.

7. J. P. Perdew and Y. Wang, *Phys. Rev. B*, 1992, **45**, 13244-13249.

8. H. J. Monkhorst and J. D. Pack, *Phys. Rev. B*, 1976, **13**, 5188-5192.

9. J. Ran, G. Gao, F. T. Li, T. Y. Ma, A. Du and S. Z. Qiao, *Nat Commun*, 2017, **8**, 13907.

10. B. Hinnemann, P. G. Moses, J. Bonde, K. P. Jorgensen, J. H. Nielsen, S. Horch, I. Chorkendorff and J. K. Norskov, *J. Am. Chem. Soc.*, 2005, **127**, 5308-5309.

11. Y. Wu, Q. Wu, Q. Zhang, Z. Lou, K. Liu, Y. Ma, Z. Wang, Z. Zheng, H. Cheng, Y. Liu, Y. Dai, B. Huang, P. Wang, *Energy Environ. Sci*., **2022**, *15*, 1271-1281.

12. F. Wang, X. Liu, Z. Zhang, S. Min, *Chem. Commun*., **2020**, *56*, 3281-3284.

13. Y.-H. Chen, J.-K. Ye, Y.-J. Chang, T.-W. Liu, Y.-H. Chuang, W.-R. Liu, S.-H. Liu, Y.-C. Pu, *Appl. Catal. B: Environ*. **2021**, *284*, 119751.